Available online at www.sciencedirect.com
ScienceDirect
Journal of the European Ceramic Society 26 (2006) 3675–3679
www.elsevier.com/locate/jeurceramsoc

Nanocrystalline orthoferrite powders: Synthesis and magnetic properties

M. Rajendran, A.K. Bhattacharya *

Warwick Process Technology Group, School of Engineering, University of Warwick, Coventry CV4 7AL, UK

Received 27 June 2004; received in revised form 11 January 2006; accepted 13 January 2006
Available online 15 March 2006

Abstract

Nanocrystalline orthoferrite powders were synthesised at low temperatures by employing an aqueous sol–gel process. Colloidal sols and water re-dispersible gels of orthoferrite precursors were prepared by room-temperature processing of inexpensive metal salts. The average diameter (Z_{av}) of the precursor particles was in the size range from 4 to 7 nm; the diameters had a narrow size distribution. Water re-dispersible translucent gel monoliths were obtained by concentrating the aqueous sols followed by drying them under reduced pressure (10^{-2} Torr) at room temperature. The sol–gel transition was found to be completely reversible. Nanocrystalline fine powders of orthoferrites of general formula, $LnFeO_3$ (Ln = La, Sm, Gd, Dy, Er, Yb and Y) having a crystallite size of about 25 nm were prepared by heating the gel precursors at 650–700 °C in air. Powder X-ray diffraction and thermogravimetry, respectively, were employed to identify perovskite phase formation and delineate thermal events that lead to gel to crystallite conversion. Magnetic measurements were carried out on the resultant powders at room temperature and down to 40 K. Nanocrystalline orthoferrite powders exhibited weak ferromagnetic behaviour, and reduced magnetic moments.

Keywords: $LaFeO_3$; Ferrites; Magnetic properties; Sol–gel processes; Nanocrystalline powders

1. Introduction

The rare earth orthoferrites crystallise in the perovskite structure and find applications in various areas such as solid oxide fuel cells, sensors and catalysis.[1–5] Fine powders of orthoferrites are desirable for these applications which can be prepared by coprecipitation,[6] by the oxalate,[7] citrate,[8] and sol–gel process[9] and by other methods.[10,11] The chemical methods offer advantages such as low-temperature oxide formation, high surface area, small particle size, exact cation-stoichiometry and phase purity.[12–14] Wet-chemical methods are promising to produce nanoparticles having discrete sizes and narrow size-distribution.

Among these, the sol–gel process is attractive since the process parameters can be varied to produce oxide powders possessing a range of desirable properties. Normally, metal alkoxides or heterometal alkoxides are dissolved in an organic solvent such as alcohol and hydrolysed under controlled conditions to produce a sol. It is essential that the hydrolysis and the condensation steps lead to bonding between two or more dissimilar metal ions via oxo or hydroxo bridging groups. This molecular level cation mixing is retained during the course of the sol–gel transition as well as on heating the gel resulting in the formation of the corresponding metal oxide at low temperatures.

However, metal alkoxides and organic solvents are expensive making the process suitable only for speciality applications, small-scale preparations and exploratory work. The moisture sensitivity of metal alkoxides, the recovery of organic solvents for reuse, handling and environmental issues make the all-alkoxide sol–gel process less attractive for large scale applications. In addition, the low solubility of rare earth alkoxides in alcohols, and the need for producing single source Ln(III)–Fe(III) precursors make the metal–organic approach relatively process intensive.

In this paper we report a novel all-inorganic aqueous sol–gel process to produce nanocrystalline orthoferrite powders at low temperatures. The process described can be easily scaled up making the process commercially viable. In addition, the magnetic properties of these nanosized powders have also been surveyed and the results are presented.

* Corresponding author. Tel.: +44 2476 524 201; fax: +44 2476 528 998.
E-mail address: akb@warwick.ac.uk (A.K. Bhattacharya).

0955-2219/$ – see front matter © 2006 Elsevier Ltd. All rights reserved.
doi:10.1016/j.jeurceramsoc.2006.01.008

2. Experimental

2.1. Sol–gel synthesis of orthoferrite precursors

A 200 mL quantity of 0.2 M aqueous solution of lanthanum nitrate, $La(NO_3)_3{\cdot}9H_2O$ (99.99%, Aldrich) was mixed with 200 mL of 0.2 M iron(III) nitrate, $Fe(NO_3)_3{\cdot}9H_2O$ (99.99+%, Aldrich) and titrated with 5% aqueous ammonia solution with constant stirring (300 rpm) at room temperature until complete precipitation of lanthanum and iron as mixed hydroxides took place. The precipitate was filtered, washed with water and peptised with 2N HNO_3 at 40 °C to get a clear sol. The resultant sol was centrifuged at 4000 rpm for 15 min to eliminate traces of unpeptised precipitate. The sol was concentrated under a reduced pressure (10^{-2} Torr) at room temperature to form a viscous sol, transferred to a petri-dish and allowed to dry at room temperature to a redispersible, monolithic translucent gel. Following the same procedure orthoferrite precursors with Sm, Gd, Dy, Er, Yb and Y, respectively, were produced by employing corresponding metal nitrates (99.99% purity, Aldrich).

2.2. Characterisation

2.2.1. Photon correlation spectroscopy(PCS) measurements

The sols were characterised for their particle size and size distribution using a photon correlation spectrometer (PCS), Malvern Instruments (Lo-C Autosizer, series 7132 multi-8 correlator) using a 4 mW diode laser, 670 nm wavelength light source. A drop of the sol was diluted with doubly distilled water to millimolar concentration, filtered through 0.2 μm filter and used for these PCS measurements.

2.2.2. Powder X-ray diffraction measurements

The crystallinity, crystal structure and phase composition of the powders were charaterised by Philips X-ray diffractometer model PW1710 using Cu Kα radiation. The spectra were recorded in the region of $2\theta = 10$–90° with a step scan of 0.1° per minute and the cell parameters were calculated and further refined using linear regression procedures (Philips APD 1700 software). The crystallite size was determined from the XRD reflection employing the following relation:

$$D_{hkl} = \frac{0.9\lambda}{\beta_{1/2}\cos\theta},$$

where D_{hkl} is the crystallite size, λ is the wavelength of Cu Kα radiation, $\beta_{1/2}$ is the calibrated half-width of the strongest reflection, and θ is the diffraction angle of that peak.

2.2.3. Magnetic measurements

For magnetic measurements a 5T Quantum Design MPMS-5S SQUID magnetometer was used. The magnetisation measurements were performed in the temperature range 40–300 K. The measurements were carried out by applying a field of 11.6 kOe and the samples were cooled from 300 K.

2.2.4. Thermal analysis

Simultaneous differential thermal analysis and thermogravimetric analysis (DTA–TGA) was performed on vacuum dried gel samples using an STA 1500 (Rheometric Scientific Ltd) in static air up to 1273 K at a ramp rate of 10 K min^{-1}.

3. Results and discussion

The size of particles in the aqueous dispersion was in the range from 4 to 7 nm and had an average size (Z_{av}) of about 6 nm. The PCS spectra of representative sols are given in Fig. 1. It is clearly seen from the figure that the size distribution falls well within the narrow range of 4–7 nm with Z_{av} of 6 nm. The sols having 3–4 wt.% solid were stable for a period of 4 weeks, and the PCS spectra remained unchanged. The PCS results are summarised in Table 1. The precursor sols upon concentration under reduced pressure (10^{-2} Torr) at room temperature resulted in a sol–gel transition to give a monolithic translucent gel. The gel was re-dispersible in water and the sol–gel transition was found to be completely reversible. Aqueous dispersions having 3–4 wt.% solid were prepared, and the diluted sols were characterised. The pH of these sols were in the range of 4.3–3.7, and addition of electrolytes or any change in pH out of this range destabilised the sols.

Thermogravimetric (TG) and differential thermal analysis (DTA) curves of a representative $YbFeO_3$ precursor gel is shown in Fig. 2. The TGA–DTA curves reveal that the formation of $YbFeO_3$ proceeds through three major thermal events—dehydration, dehydroxylation and final dehydroxylation process to give a constant mass. These major thermal events are shown as strong and relatively broad endotherms centred around 100, 185 and 305 °C, respectively. There is a broad overlapping endotherm that extends beyond 450 °C. There is one to one correspondence to the thermal events and the TG-weight loss steps. The endotherm around 100 °C and the further weak endotherm at 185 °C correspond to the elimination of surface bound water from the gel. The subsequent endotherms at

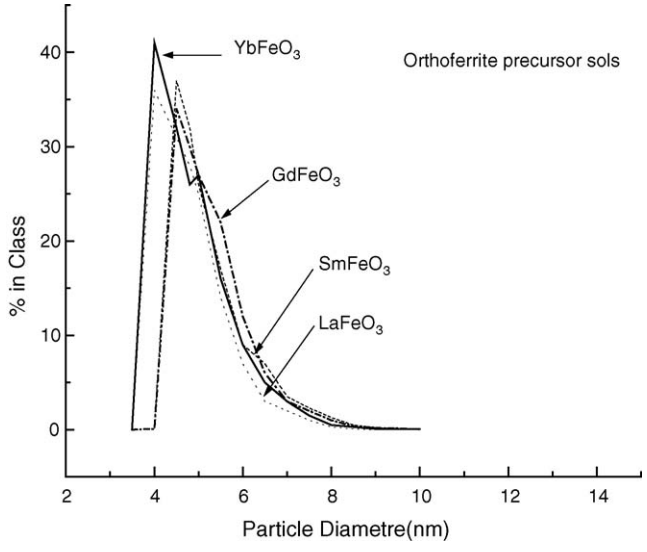

Fig. 1. Photon correlation spectra of $LnFeO_3$ precursor sols.

Table 1
Characteristics of the precursor sols, structure and magnetic properties of the nanocrystalline orthoferrite powders

Compound	Sol partical size (nm)	Unit cell parameter (Å)			Unit cell volume (Å^3)	Magnetic moments (emu mol^{-1})	
		a	*b*	*c*		Nano	Coarse
$LaFeO_3$	6.3	5.555	5.565	7.863	243.1	243	255
$SmFeO_3$	6.0	5.394	5.593	7.712	232.7	217	230
$GdFeO_3$	6.0	5.347	5.615	7.668	230.2	254	273
$DyFeO_3$	5.8	5.303	5.599	7.622	226.3	210	225
$ErFeO_3$	5.5	5.264	5.583	7.594	223.2	220	228
$YFeO_3$	6.0	5.286	5.594	7.606	224.9	–	–
$YbFeO_3$	5.6	5.235	5.556	7.571	220.1	241	250

305 °C and the broad endotherm extending to 450 °C represent major events occurring as a result of the break-up of the gel net work. The events represent the dehydroxylation process, wherein hydroxo groups (–M–O(H)–M–O(H)–) both bridging and non-bridging are converted into oxo groups (M–O–M–O–) by condensation. Thermogram (TG) shows a constant weight at 450 °C after an overall weight-loss of 41.3%. The powder XRD of the solid residue obtained at this stage revealed that it was amorphous but crystallised to perovskite structure on heating above 650 °C. The weak exotherm at 650 °C, therefore, corresponds to the crystallisation of the $YbFeO_3$ to perovskite structure.

The powder X-ray diffraction pattern of the orthoferrite precursor gels showed that they were amorphous. The gels were then heated to increasingly higher temperatures and the XRD patterns were recorded. Fig. 3 shows typical XRD patterns of $LnFeO_3$ (Ln = La and Yb) produced from corresponding precursor gels heated to 700 °C. The XRD patterns of the orthoferrites having the largest rare earth ion (La^{3+}) and the smallest rare earth ion (Yb^{3+}) are shown in the figure. Heating to 600 °C showed the onset of crystallisation with the appearance of a few reflections. Further heating to 650–700 °C resulted in complete crysallisation of the perovskite phase for all orthoferrites, and the extreme members are shown in the Fig. 3. Prominent reflections of the perovskite structure appeared in the region, $2\theta = 30$–$35°$ on heating and all the reflections of the corresponding perovskite structure were identified. It is clear from the XRD patterns that the samples are single phase perovskite oxides, which are free from impurity phases. The crystalline orthoferrite phase formed directly without any phase segregation into rare earth oxide and iron oxide from the amorphous phase. This suggests that in the all-inorganic sol–gel process, molecular level mixing of metal ions is retained at various stages of processing to enable the formation of the desired compounds at relatively low temperatures of 650–700 °C. A crystallite size of about 25 ± 2 nm is determined from the prominent XRD reflection for all the samples that were heated to 700 °C for 1 h. Since the molecular precursor approach overcomes the diffusional and phase boundary constraints normally associated with solid state reactions, all these compounds are formed at low temperatures and require only short heating duration of about 1 h. From the XRD patterns unit cell parameters were determined and the values are listed in Table 1. The unit cell parameters are in good agreement with the literature.[15]

Fig. 4 shows the variation of lattice parameters as a function of rare earth ionic size. As seen from the figure, '*a*' and '*c*' parameters decrease smoothly for rare earth ions of smaller size. As expected the unit cell volume decreases gradually from $LaFeO_3$ to $YbFeO_3$. However, the '*b*' parameter shows unexpected

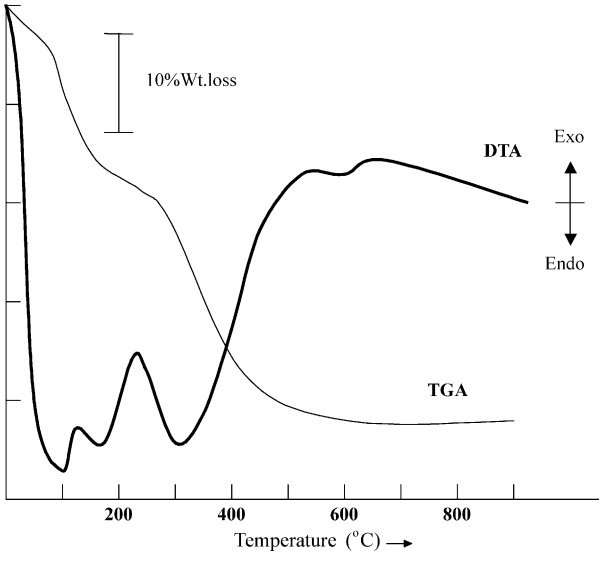

Fig. 2. TG–DTA trace of re-dispersible $YbFeO_3$ precursor gel.

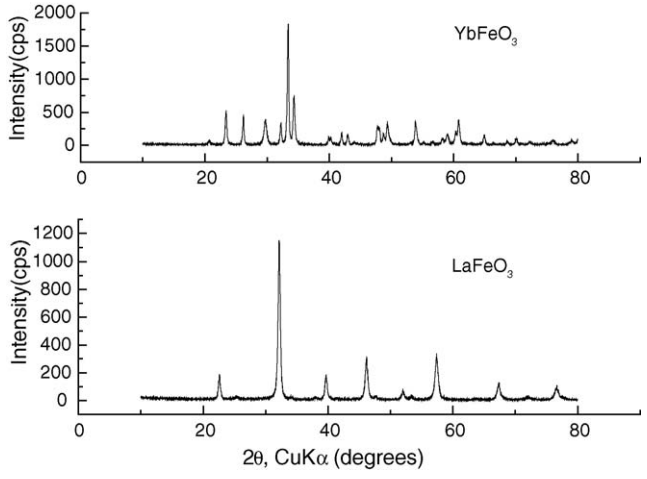

Fig. 3. Typical powder X-ray diffraction patterns of nanocrystalline $LaFeO_3$ and $YbFeO_3$ powders.

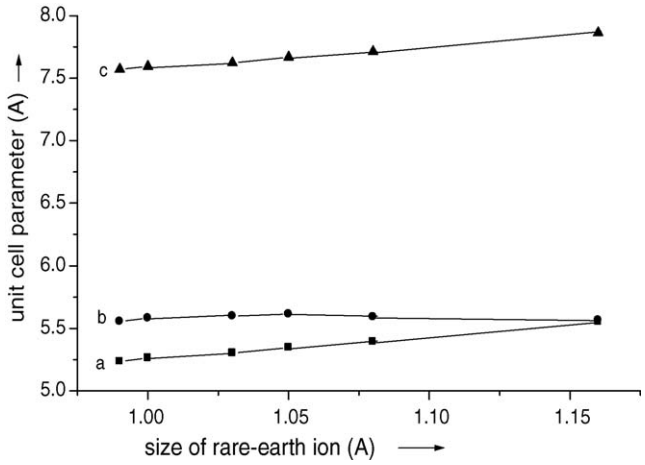

Fig. 4. Variation of unit cell parameters as a function of rare earth ionic size for aqueous sol–gel derived orthoferrites powders.

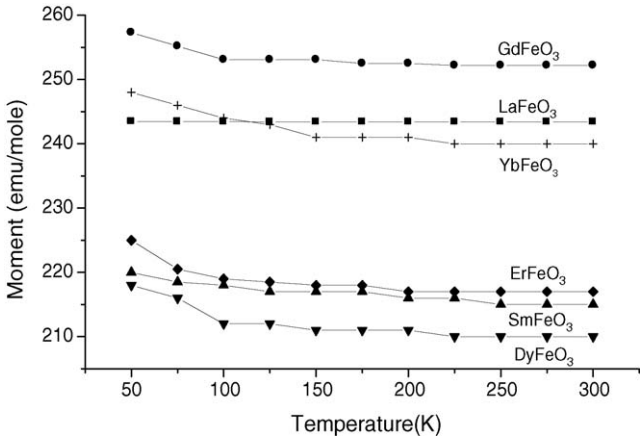

Fig. 6. Magnetisation vs. temperature measurements for nanocrystalline orthoferrite powders.

behaviour as it goes through a maximum at about Dy^{3+}–Gd^{3+} but decreases from Gd^{3+} to Yb^{3+}. These structural variations are the result of the size mismatch between the trivalent rare earth and Fe^{3+} ions distorting the perovskite lattice to give optimum coordination to Ln ions.[15,16] The Ln–O bond length is enlarged by a cooperative buckling of corner shared FeO_6 octahedra to match the Fe–O bond length. The buckling of FeO_6 octahedral units results in a decreased cation–oxygen–cation bond angle from 180° and the orthoferrites having smaller rare earth ions, therefore adopt the space group Pbnm, while the compounds having larger rare earth ions crystallise in Pnma.

Fig. 5 is the *M–H* curve obtained for 25 nm sized $LaFeO_3$ powders showing weak ferromagnetic behaviour at room temperature. The magnetisation does not saturate even at high fields of 60 kOe, and the moment values are considerably lower than those reported in the literature.[16,17] This could be due to the large surface to volume ratio of the nanocrystalline powders. Table 1 summarises the room temperature magnetic properties of $LaFeO_3$ and other ferrites.

The temperature dependent magnetisation behaviour of nanocrystalline orthoferrite powders are shown in Fig. 6. As it is clearly seen all the orthoferrites exhibit weak ferromagnetic behaviour at room temperature and it persists down to 40 K. The orthoferrites are essentially antiferromagnetic, and the faint ferromagnetic response given by these oxides is of considerable interest.[18,19] The magnetic sub-structure in orthoferrites can be described by two interpenetrating pseudo-cubic face centred sub-lattices in which each Fe^{3+} ion is surrounded by six nearest neighbour Fe^{3+} ions. The crystal structure is deformed considerably from the ideal perovskite structure and the FeO_6 octahedra are tilted to varying degrees depending on the size of the rare earth ion. This results in non-collinear arrangement of the two magnetic sub-lattices to a residual moment, and the magnitude depends on the angle of spin-canting which is about 0.5°. The room temperature moments are found to lie approximately parallel to the [0 0 1] axis.[20] In nanocrystalline samples, the large surface to volume ratios are known to influence the magnetic properties.[21]

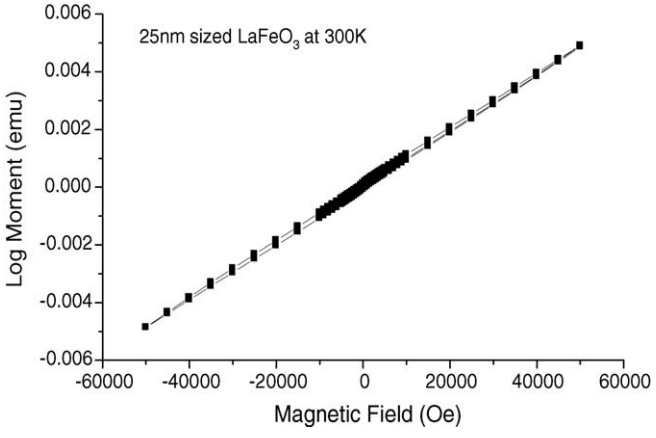

Fig. 5. *M–H* curve for 25 nm $LaFeO_3$ at room temperature.

Therefore, the moment is intrinsic to the sample, and it is essentially due to canting in the alignment of the two antiferromagnetically coupled lattices in the distorted perovskite structute. This canting is sufficient to give a small net ferromagnetic moment perpendicular to the antoferromagnetic axis. At 300 K, the moments range from 210 to 256 emu mol^{-1}, and $DyFeO_3$ and $GdFeO_3$, respectively, showed the lowest and the highest values. $LaFeO_3$ showed almost the same moment down to 40 K, whereas for the other ferrites it increased slightly below 75 K. The magnetisation measurements are in agreement with earlier reports, but the moments are relatively lower and the values are given in Table 1.[16,17]

It is worth comparing the weak spontaneous magnetic moments observed in orthoferrites to other such magnetic systems. A moment of 57.6 emu mol^{-1} is reported for α-Fe_2O_3,[22] and 188 emu mol^{-1} for $MnCO_3$.[23] The ferromagnetic moment distribution is found to deviate from spherical symmetry for these compounds. For nanocrystalline orthoferrites the room temperature moment values range from 210 to 256 emu mol^{-1}, which are somewhat lower compared to the coarse grained samples prepared by conventional methods.

4. Conclusions

In this paper it is shown that nanocrystalline orthoferrite powders can be prepared by an inexpensive aqueous inorganic sol–gel process. The sol–gel transition is completely reversible. Crystalline orthoferrites were formed at a relatively low temperature of 650 °C without any phase segregation to individual rare earth oxide and iron oxide. The perovskite phase was formed directly from the gel precursor without any crystalline phase segregation. The process described can be readily scaled up making the process commercially viable. The resultant nanocrystalline orthoferrites exhibited weak ferromagnetic behavior, and reduced moments.

References

1. Ueda, K., Tabata, H. and Kawai, T., *Jpn. J. Appl. Phys.*, 1999, **38**(Pt 1), 6690.
2. Kahn, F. J., Pershan, P. S. and Remeika, J. P., *Phys. Rev. Lett.*, 1969, **186**, 891.
3. Belessi, V. C., Trikalitis, P. N., Ladavos, A. K., Bakas, T. V. and Pomonis, P. J., *Appl. Catal. A*, 1999, **177**, 53.
4. Huang, K., Lee, H. Y. and Goodenough, J. B., *J. Electrochem. Soc.*, 1999, **145**, 3220.
5. Traversa, E., Villanti, S., Gusmano, G., Aono, H. and Sadaka, Y., *J. Am. Ceram. Soc.*, 1999, **82**, 2442.
6. Li, X., Zhang, H. B. and Zhao, M. Y., *Mater. Chem. Phys.*, 1994, **37**(2), 132.
7. Usha, M. G., Subba Rao, M. and Kutty, T. R. N., *Thermochim. Acta*, 1981, **43**(1), 35.
8. Anderton, D. J. and Sale, F. R., *Powder Metall.*, 1979, **22**, 14.
9. Vazquez-Vazquez, C., Kogerler, P., Lopez-Quintela, M. A., Sanchez, R. D. and Rivas, J., *J. Mater. Res.*, 1998, **13**(2), 451.
10. Aono, H., Ohmori, J. and Sadaoka, Y., *J. Ceram. Soc. Jpn.*, 2000, **108**(10), 892.
11. Xiong, G., Yang, X. J., Lu, L. D. and Wang, X., *J. Inorg. Mater.*, 1998, **13**(4), 613.
12. Rajendran, M. and Rao, M. S., *J. Solid State Chem.*, 1994, **113**, 239.
13. Matijevic, E., In *Chemical Processing of Advanced Materials*, ed. L. L. Hench and J. K. West. Wiley, New York, 1992, pp. 513–527.
14. Rajendran, M. and Bhattacharya, A. K., *Mater. Sci. Eng. B*, 1999, **60**, 217.
15. Goodenough, J. B. and Longo, J. M., *Magnetic Oxides and Related Compounds, Part a, Vol. III/4a, LB New Series*. Springer-verlag, New York, 1970, p. 126.
16. Tebble, R. S. and Craik, D. J., *Magnetic Materials*. Wiley-Interscience, London, 1969, pp. 338–356.
17. Yamamura, H., Shirasaki, S. I., Oshima, H. and Kakegawa, K., *J. Solid State Chem.*, 1976, **18**, 329.
18. Mathur, S., Veith, M., Rapalavicuite, R., Shen, H., Goya, G. F., Filho, W. L. M. and Berquo, T. S., *Chem. Mater.*, 2004, **16**(10), 1906–1913.
19. Mathur, S., Shen, H., Lecerf, N., Kjekshus, A., Fjellvag, H. and Goya, G. F., *Adv. Mater.*, 2002, **14**(19), 1405.
20. Tofield, B. C. and Fender, B. E. F., *J. Phys. Chem. Solids*, 1970, **31**, 2741.
21. Rajendran, M., Pullar, R. P., Bhattacharya, A. K., Das, D., Chintalapudi, S. N. and Majumdar, C. K., *J. Magn. Magn. Mater.*, 2001, **232**(1–2), 71–83.
22. Nathans, R., Pickart, S. J., Alperin, H. A. and Brown, P. J., *Phys. Rev. A*, 1964, **136**, 1641.
23. Brown, P. J. and Forsyth, J. B., *Proc. Phys. Soc.*, 1967, **92**, 125.